Electrical Input Filters of Ganglion Cells in Wild Type and Degenerating rd10 Mouse Retina as a Template for Selective Electrical Stimulation

Hamed Shabani, Eberhart Zrenner, Daniel L. Rathbun, *Member, IEEE*, and Zohreh Hosseinzadeh

***Abstract*— Bionic vision systems are currently limited by indiscriminate activation of all retinal ganglion cells (RGCs) – despite the dozens of known RGC types which each encode a different visual message. Here, we use spike-triggered averaging to explore how electrical responsiveness varies across RGC types toward the goal of using this variation to create type-selective electrical stimuli. A battery of visual stimuli and a randomly distributed sequence of electrical pulses were delivered to healthy and degenerating (4-week-old rd10) mouse retinas. Ganglion cell spike trains were recorded during stimulation using a 60-channel microelectrode array. Hierarchical clustering divided the recorded RGC populations according to their visual and electrical response patterns. Novel electrical stimuli were presented to assess type-specific selectivity. In healthy retinas, responses fell into 35 visual patterns and 14 electrical patterns. In degenerating retinas, responses fell into 12 visual and 23 electrical patterns. Few correspondences between electrical and visual response patterns were found except for the known correspondence of ON visual type with upward deflecting electrical type and OFF cells with downward electrical profiles. Further refinement of the approach presented here may yet yield the elusive nuances necessary for type-selective stimulation. This study greatly deepens our understanding of electrical input filters in the context of detailed visual response characterization and includes the most complete examination yet of degenerating electrical input filters.**

***Index Terms*— Neural implants, neural prosthesis, neuroprostheses, visual prosthesis.**

Manuscript received 16 June 2023; revised 14 October 2023 and 19 December 2023; accepted 18 January 2024. Date of publication 31 January 2024; date of current version 22 February 2024. The work of Daniel L. Rathbun was supported by Bundesministerium für Bildung und Forschung under Grant 031a308. The work of Zohreh Hosseinzadeh was supported in part by Deutsche Forschungsgemeinschaft under Grant HO 6221/1-1, in part by PRO RETINA under Grant Pro-Re/KP/Hosseinzadeh.1-2020, in part by European Research Council (ERC) under Grant 101039764, and in part by the Tistou and Charlotte Kerstan Foundation. *(Corresponding author: Daniel L. Rathbun.)*

This work involved human subjects or animals in its research. Approval of all ethical and experimental procedures and protocols was granted by the Tübingen University committee on animal protection, Einrichtung für Tierschutz, Tierärztlicher Dienst und Labortierkunde.

Hamed Shabani is with the Theoretical Systems Neuroscience, Bernstein Center Freiburg, University of Freiburg, 79104 Freiburg, Germany (e-mail: hamed.shabani@bcf.uni-freiburg.de).

Eberhart Zrenner is with the Institute for Ophthalmic Research, Centre for Ophthalmology, Eberhard Karls University, 72076 Tübingen, Germany (e-mail: ezrenner@uni-tuebingen.de).

Daniel L. Rathbun is with the Detroit Institute of Ophthalmology, Department of Ophthalmology, Henry Ford Health, Detroit, MI 48202 USA (e-mail: drathbu2@hfhs.org).

Zohreh Hosseinzadeh is with the Department of Ophthalmology, Radboud University Medical Center, 6525 GA Nijmegen, The Netherlands, and also with the Department of Ophthalmology and Eye Hospital, Leipzig University, 04109 Leipzig, Germany (e-mail: Zohreh.Hosseinzadeh@medizin.uni-leipzig.de).

This article has supplementary downloadable material available at https://doi.org/10.1109/TNSRE.2024.3360890, provided by the authors.

Digital Object Identifier 10.1109/TNSRE.2024.3360890

I. Introduction

DURING the last few decades, successful efforts have restored limited vision to patients with progressive retinal degenerative diseases such as retinitis pigmentosa and age-related macular degeneration by electrically stimulating the retina [1]. Leading implants include the Argus II epiretinal implant of Second Sight Medical Products, Inc., Sylmar California, USA [2], the IRIS II epiretinal implant of Pixium Vision, Paris, France [3] and the Alpha AMS subretinal device from Retina Implant, GmbH, developed in Tübingen, Germany [4] which have each received regulatory approval and been sold commercially.

Despite these successes of retinal implants, it remains necessary to refine our understanding of signal processing through the implant-stimulated retina in the interest of improving visual percepts for implanted patients. Only recently has it become possible to differentiate between the dozens of distinct types of retinal ganglion cells (RGCs) which each convey their own visual information to the brain. Catalogs of differentiated RGCs have been achieved through state-of-the art techniques including 47 morphological types [5], 40 genetic types [6], 28 physiological types using spike train data [7], 45 types based on scRNA-seq [8], 32 types using calcium signal data [9]. With these catalogs now available, a next step is to use the most applicable amongst them to understand how responses to electrical stimulation differ between the various types. The main purpose of this study is to develop cell type-selective stimulation by examining spiking responses to the novel electrical noise stimulus in the context of these newly-refined visual response catalogs.

Many researchers have explored electrical stimulation parameters for preferential activation of one retina ganglion cell (RGC) type over another. The broadly defined ON and OFF RGC types respond to different phases of a low frequency sine wave [10], [11]. Similarly, Twyford et al. [12] also

© 2024 The Authors. This work is licensed under a Creative Commons Attribution 4.0 License.
For more information, see https://creativecommons.org/licenses/by/4.0/

showed that an amplitude-modulated pulse train envelope could differentially activate RGCs through direct stimulation, e.g. ON cells with decreased activity and OFF cells with increased activity. Other recent contributions to growing evidence of cell-type selective stimulation include [13], [14], [15], [16], [17], [18], [19].

In contrast to such parametric approaches, the method of white noise stimulation, paired with reverse correlation of response to stimulus (examined in [20]) allows each neuron to select out its optimal stimulus from a broad field of potential stimuli without those stimulus patterns being explicitly presented. We previously leveraged this white noise method to estimate the electrical input filters of mouse RGCs via indirect stimulation of the retinal network [21]. Because the estimate is achieved by the reverse-correlation technique of spike-triggered averaging of electrical pulse sequences, we designated it the electrical Spike Triggered Average (eSTA). Subsequently, we demonstrated that there is a correspondence between visual and electrical input filters of ON and OFF mouse retinal ganglion cells [22]. As confirmed by Ho et al. [23] ON cells have a characteristic upward deflection of eSTA, whereas OFF cells have a downward deflection. This dichotomy echoes the finding that ON and OFF cells respond to different phases of an ongoing sine wave [10]. This dichotomy likely exists because the retinal element that is most strongly activated by such stimulation precedes a signal inverting split between ON and OFF pathways (e.g., photoreceptors or A-II amacrine cells, discussed in [22]).

Most recently, we attempted to benchmark eSTA differences with an established catalog of RGC types based on functional responses to light stimulation [24]. Owing to the difficulty of precisely connecting spike trains with calcium imaged signals, this attempt met with only qualified success. Therefore, we conducted the present study to build on this earlier work of comparing the electrical input filters of different RGC types to their visual responses. Our hope has been that clear eSTA differences between RGC types can be used to design electrical stimuli to target selectively RGC types.

Here, we have expanded on our previous work by using type boundaries that are best matched to our data. We have clustered RGCs of healthy and rd10 degenerated retinas using either visual responses to light stimulation or eSTA shapes. This study presents 35 visual patterns and 14 electrical patterns of healthy mouse retina as well as 12 visual and 23 electrical patterns of degenerating rd10 retina. This experimental approach presented here constitutes a significant elaboration upon prior methods, and a significant contribution to bionic vision in the effort to design new electrical stimuli that can selectively activate RGC types.

In parallel to these main experiments, we have begun testing 4 types of electrical stimuli where the pulse train is modulated by either half or full sinusoids. These correspond to our earlier observations that the broad RGC categories of ON and OFF cells have stereotypically upward or downward eSTA shapes, respectively. Unsurprisingly, given the heterogeneity of the broad ON and OFF classifications, we found a range of selectivity for these sinusoids that generally confirm expectations. Rather than wait until this puzzle is fully resolved, we present these preliminary results to hasten that resolution.

II. Methods

A. Animals

Male and female adult wild type (WT) mice C57Bl/6J (The Jackson Laboratory, Bar Harbor, ME, USA) with age ranging from postnatal day 29 to 74 and rd10 (on a C57Bl/6J background, The Jackson Laboratory) mice from 29 to 31 postnatal days were used for this study. Since the photoreceptor layer is not completely degenerated at this age they can be considered as a proper model for progressive Retinitis Pigmentosa in the stage where some neurons still respond to light stimulation. Before each experiment, animals were housed under standard lighting conditions with free access to food and water. All procedures were done in accordance with the ARVO statement for the use of animals in ophthalmic and visual research; and experiments were approved by the Tübingen University committee on animal protection (Einrichtung für Tierschutz, Tierärztlicher Dienst und Labortierkunde).

B. Retinal Preparation

Animals were dark-adapted for at least one hour before each experiment and anesthetized with Isoflurane before cervical dislocation. The absence of withdrawal reflex was checked by pinching the tissue between the toes before euthanasia. The eyes were removed and dissected under dim red light in carbogenated (95% O2 and 5% CO2) artificial cerebrospinal fluid (ACSF) solution containing the following (in mM): 125 NaCl, 2.5 KCl, 2 CaCl2, 1 MgCl2, 1.25 NaH2PO4, 26 NaHCO3, and 20 Glucose, pH 7.4. The retina was detached from the pigment epithelium, after removing the cornea, ora serrata, lens and vitreous body from the eye. Half or whole retina was then placed carefully on the planar microelectrode array (MEA) in a way that the ganglion side faces the electrodes. A dialysis membrane (CelluSep, Membrane Filtration Products Inc., Seguin, Texas, USA) mounted on a custom Teflon ring was placed on the MEA to keep the retina immovable and in contact with electrodes while letting the carbogenated ACSF reach the tissue [25], [26]. After connecting the preamplifier to the MEA, the retina was continuously perfused with carbogenated ACSF at ∼3 ml/min rate and maintained at 33°C using both a heating plate and a heated perfusion cannula (HE-Inv-8, PH01, Multi Channel Systems, Reutlingen, Germany). At least 30 min of stabilization time was observed before each recording.

C. MEA Recording

A 60-channel planar MEA with an 8∗8 rectangular layout (60MEA200/30iR-ITO, Multi Channel Systems, Reutlingen, Germany) was used for recording the extracellular activity of RGCs. The MEA was connected to a preamplifier (MEA 1060-Inv-BC) located on the setup rig with a gain of 53x. The output of the preamp was connected to the next amplifier with the gain of 21x and an analog to digital converter, with separate inputs on the recording computer data acquisition card for stimulus triggers. The MC_Rack program developed by

Multi Channel Systems was used for the collection and online visualization of data. Raw data were recorded with the rate of 50 kHz/channel using the Multi Channel Systems amplifiers with a total gain of 1100 using a filter with bandwidth of 1Hz to 3 KHz.

D. Spike Detection and Preprocessing

A commercial spike sorting software (Offline Sorter, Plexon Inc., TX, USA) was used to detect and sort spike events. Raw data were filtered with a second-order 300 Hz high pass Bessel filter. Spike events then were detected by using a simple threshold crossing algorithm by which the negative deflections below 5 standard deviations of mean were considered as an event. Spike sorting was performed using the T-distribution Expectation-Maximization algorithm and the final sorting solution was determined manually by visual inspection of spike grouping quality [21], [25]. The NeuroExplorer program (Plexon Inc., TX, USA) was used to export spike timestamps into MATLAB (The Mathworks, Natick, MA) for final analysis.

E. Visual and Electrical Stimulation

The visual stimulation set was adapted from Baden et al. [9] and customized for MEA implementation [27], [28]. The stimuli consist of a set of 1000 $\times$ 300 μm moving bars sweeping over the MEA surface in eight directions (up, down, left, right, and the 4 diagonals) with vertical bars at 15 locations, horizontal bars at 10 locations, and diagonal bars at 17 locations for each diagonal axis, with the centers of adjacent locations separated by 200 μm; a set of full-field contrast and temporal frequency chirps, consisting of two sinusoidal intensity modulations, one with increasing frequency up to 8 Hz and one with increasing contrast; black and white flash (2 s white and 2 s black); and blue-green color flashes for 3 s each in a sequence of blue, black, green, black. For light stimulation, we focused a developer module projector (DLP® LightCrafter 4500, Texas Instruments) through a custom light path of lens, mirror, and condenser onto the MEA. Stimulator intensity (as photoisomerization rate, P$*$/s/cone) was calibrated to match the previous Baden e al. [9] study as closely as possible, with the white stimulus set to 3×104 P$*$/s/cone photoisomerization rage for mouse UV- and M-cones and the black stimulus set to 104 P$*$/s/cone. A steady mean illumination 2 $\times$ 104 P$*$/s/cone was present during, before, and after all electrical and visual stimuli to maintain adaptation state.

The electrical stimulation was delivered epiretinally after visual stimulation. Although network activation is typically the goal of subretinal implants which stimulate from the photoreceptor side of the retina, network activation can be achieved at reasonable thresholds by stimulating from either side of the retina. The electrical white noise stimulus was a 25 Hz train of monophasic, rectangular, cathodic voltage pulses with 1 ms width selected with replacement from a Gaussian distribution of amplitudes with a mean of -800 mV and standard deviation of 35% (280 mV). The electrical noise stimulus was delivered to the MEA using an STG 4008 stimulus generator (MCS, Reutlingen, Germany). This stimulus protocol has previously been shown to be effective in estimating integrative electrical input filters of the type examined here [21], [22]. The electrical charge was delivered to tissue via one of the 59 recording electrodes of the MEA - chosen based on proximity to electrodes with robust light-induced activity. In these experiments, electrically stimulated cells were recorded on all electrodes of the MEA. Accordingly, the distance between stimulating electrode and stimulated cell ranged up to 1 mm. No eSTA parameters were found to vary systematically with distance from stimulating electrode, therefore, all distances were grouped for analysis. The duration of each identical trial was 100 s. For electrical noise analysis, a spike latency exclusion period of 10 ms was applied to remove the influence of direct RGC activation on our results. The number of trial repetitions varied from 15 to 30 across different experiments - depending on available recording time.

F. ON/OFF Index

The ON/OFF index was computed for each cell based on the full field flash stimulus. This index quantifies the preference of each cell for onset vs. offset of light by comparing the maximum firing rate of light and dark periods. We computed the ON/OFF index as follows:

$$\mathrm{OOi} = (\mathrm{A_{ON}}) - (\mathrm{A_{OFF}})/(\mathrm{A_{ON}}) + (\mathrm{A_{OFF}}) \quad (1)$$

where ($\mathrm{AR_{ON}}$) and ($\mathrm{AR_{OFF}}$) are peak amplitudes of the response PSTH during light on and light off periods, respectively. The output of this formula is a number between -1 to +1 which respectively show the level of OFF and ON preference. We have not used this index for clustering, but it was considered as extra information for interpreting the clusters.

G. Direction Selectivity Index

We customized the direction selectivity index (DSi) for our drifting bar stimuli that were presented in 8 directions and along 59 paths across the MEA during experiments [27]. First, for each cell, we used responses to the 3 bars of each direction that passed closest to the cell's electrode. Because the bars began drifting at different times relative to the cell's receptive field, we aligned the times of each recording so that each bar entered the cell's receptive field at the same adjusted time. Then, for computing DSi, the relative maximum firing rate was taken for each of the 8 directions and transformed to a vector that represents each direction using 200 ms time bins [7]. The first two eigenvalues of the vector were used to compute the DSi index: DSi=1-λ1/λ2.

H. Variance Ratio

To remove noisy units with low stimulus-driven activity before clustering, we compared the response variance of chirp data with the overall variance of the recorded data during chirp stimulation. This reflects how strongly the response of each unit is modulated by the stimulus. To compute response variance, the variances across at least 10 trials of 100 ms binned spike counts was calculated, and these values were then averaged. The overall variance was calculated across the full

set of time bins and trials including both response intervals and spontaneous intervals. Cells with a response variance higher than the overall variance (a ratio higher than 1) were excluded from analysis as unreliably driven cells [24].

I. Response Clustering

No standardized method has yet been established to assign mouse RGCs into their presumed dozens of true functional types based on spiking responses to visual stimuli. Therefore, we sought to sort our data, using previously established methods, into the maximal number of visual response groups that the dataset could support [7].

We used interspike interval (ISI) and spike based (SPIKE) distance metrics for clustering of visual response spike trains [7], [29], [30], [31]. These are parameter-free measures that quantify the similarity between pairs of spike trains as a distance between the two trains. We chose these metrics from the many appropriate ones that could be used because they have previously been used in a similar application. Therefore, comparison with the earlier work will be more meaningful.

ISI and SPIKE metrics are complementary. Both have been used here to remain agnostic about the most relevant neural response features. The ISI method is especially useful with responses exhibiting diverse time scales. The SPIKE metric's utility lies in its capacity to gauge the level of coordination exhibited between neural spike occurrences. This metric proves particularly advantageous in identifying functional relationships between individual neurons.

For each stimulus and each cell pairing, distances were calculated between each pairwise combination of stimulus repetitions and averaged to produce a single distance between the two cells using the PySpike toolbox [32, version 0.5.3]. The computed matrix of pairwise cell distances then was used for hierarchical clustering by implementing the SciPy library [33, version 1.0.1] with the Ward minimization algorithm [7].

Hierarchical agglomerative clustering was implemented to construct a dendrogram ranging from each cell as its own cluster to all cells combined into a single cluster [7]. In this method, each unit is considered as a separate cluster, then iteratively, the clusters are merged according to a minimum variance constraint. To set the dendrogram cut-off point, different criteria can be used to quantify the quality of each clustering solution. The two measures used to estimate the optimal number of clusters were the gap statistic and adjusted mutual information. For the gap statistic, the distance matrix is shuffled to create a random surrogate to which each clustering solution is applied; and the dispersion of these clusters is calculated. The dissimilarity between this random surrogate's cluster dispersion and that of the unshuffled data constitutes the gap statistic. Scanning across all numbers of clusters, the clustering solution that produces the largest gap statistic is taken to represent the optimal number of clusters [7], [34]. Gap statistics can be too conservative in terms of cluster numbers for data with higher variability [7]. Therefore, we also computed the adjusted mutual information (AMI) as a consensus method between ISI and SPIKE metrics. For the AMI, the ISI- and SPIKE-based solutions are compared at each point along the clustering dendrogram. The more these solutions agree with each other above a random agreement expectation, the higher the mutual information. The clustering solution with the highest AMI was taken to represent the optimal number of clusters.

For clustering of electrical responses, the eSTA for each cell was computed; and the Euclidian distance between normalized eSTA vectors was computed for all cell pairs to yield a distance matrix. The gap statistic was then applied to agglomerative clustering solutions to identify the optimal number of clusters, as described above. Mutual information could not be applied for this clustering since eSTA vectors rather than spike trains were used.

J. Electrical Input Filter Estimation

An established method to estimate a neuron's sensitivity to complex electrical stimuli is to generate an eSTA. To obtain the eSTA, Gaussian white noise stimuli were applied to the retina. Then, the stimuli that precede each neuronal spike were averaged across all spikes, yielding an estimate of the input filter for that neuron. The MATLAB toolbox developed by Pillow et al. (https://github.com/pillowlab/LNPfitting) [35], [36] was used to generate eSTAs for the 1 s preceding and 1 s following spikes. The computed eSTA then were imported into the Python environment for further analysis. For analysis eSTAs were first smoothed with a cubic spline interpolation at 8 ms samples, and then normalized according to a z-score method by subtracting the mean and dividing by the standard deviation of the STA. Notably, we used the term 'electrical STA' to differentiate these filters from the more common visual STAs that are often referenced in the visual neurophysiology literature.

It has been reported that subthreshold stimulation leads to network-mediated activation of RGCs, sometimes characterized by burst responses with low spike-time precision [37], which could artificially broaden the width of eSTAs. To avoid this problem, we applied the burst correction algorithm proposed by Sekhar et al. [21]. Through burst correction, only the time of the first spike of a burst is considered and then the contribution of the associated stimulus is weighted by the number of spikes in that burst.

The significance of eSTAs was computed differently for wild type and rd10 data. For wild type data, we used the Python function normal test to test the null hypothesis that the 25 samples (1 s at stimulation frequency of 25 Hz) of eSTA prior time zero come from a normal distribution (alpha=0.001). Applying this test to rd10 data gave a high false-positive error due to the rhythmic oscillations of rd10 eSTAs. Therefore, we implemented a different approach in which the hypothesis that positive and negative peaks come from the same distribution as the baseline is tested using ztest in MATLAB (alpha = 0.0001) [21].

K. Electrical Sinusoid Stimulation

We have previously found a strong correspondence between the eSTA and visual response pattern for ON and OFF RGCs. In the preliminary experiment reported here, we sought to test whether electrical stimuli derived from these eSTAs could

preferentially activate ON and OFF cells. Because the eSTA represents an estimate of the best electrical stimulus for activating a cell, we designed standardized sinusoidal stimuli approximating the monophasic and biphasic eSTA shapes that were most commonly encountered (Fig. 8). These full- and half-sinusoids were embedded within ongoing cathodic pulse electrical noise so that the cells were in the same adaptational state as when the eSTAs were generated. The sinusoids were 100% modulated to range from 0 to -1600 mV, with a mean of -800 mV. For activation of ON cells, full and half sinusoids ending with an upward deflection were presented. Similarly, full- and half-sinusoids ending with a downward deflection were intended to activate OFF cells. For these 4 different shapes, 4 different temporal frequencies were presented resulting in a complete stimulus set of 16 different noise-embedded sinusoids. The frequencies of 1, 2, 3, and 4 Hz were chosen to cover the range of previously observed eSTAs.

L. Statistics

Unless otherwise noted, population data were expressed as arithmetic means ± SEM. Statistical analysis for power spectrum densities and eSTA parameters were performed using GraphPad Prism 6 software (GraphPad Software, La Jolla, CA, USA). For comparisons between groups, Student's unpaired t-test was used with an alpha < 0.05. Bimodality was tested with the Hartigan dip test.

III. Results

Our main purpose is to develop cell type-selective stimulation by examining spiking responses our electrical noise stimulus in the context of detailed visual response classification. To obtain the electrical characteristics of individual mouse RGC types, we performed agglomerative hierarchical clustering on both light- and electrically-induced responses. For visual-based clustering, the ISI and SPIKE distance matrix were computed. The temporal linear filters estimated by the eSTA were used to create alternative clusters based on the responses of RGCs to electrical Gaussian noise stimulation.

A. Clustering RGCs per Visual Responses From Healthy Retinas

The light-induced activity of 2632 detected units from 22 wild type (WT) C57Bl/6 mouse retinas, recorded with a 60-channel MEA (*Methods*) was used for clustering. Since the purpose of this study is to characterize the electrical profiles of RGCs, only cells with significant eSTAs were considered, which left 476 cells for further analysis. Additionally, low firing rate cells with the average of interspike intervals above 2 SD (standard deviation) of the population mean (during flash) were considered as outliers and removed from clustering leaving 353 cells. To ensure that analyzed responses were stimulus-driven, the Pearson correlation between stimulus and response (for flash) was computed and only cells with a correlation value higher than 0.1 were included. In addition, cells with a variance ratio (*Methods*) of 1 or higher during chirp stimulation were excluded. This yielded a total number of 295 WT cells, with 18 of the retinas contributing at least one cell for final clustering.

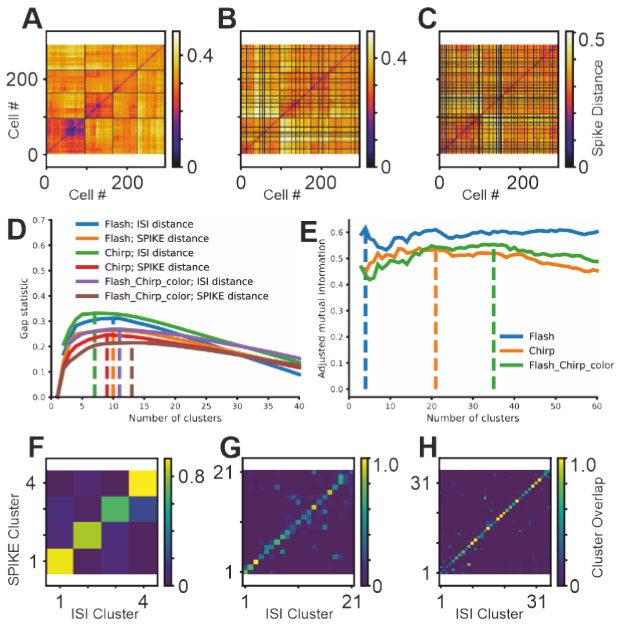

Fig. 1. **Optimization of RGC clusters from healthy retinas.** (A-C) Pairwise distance matrices for flash, chirp, and flash + chirp + color stimulus responses, respectively. SPIKE-based distances are shown. Vertical and horizontal black lines separate clusters. (D) Gap statistic scanned across cluster number for combinations of stimuli with either ISI or SPIKE-based distances. Dashed vertical lines indicate optimal cluster number. (E) Mutual information between ISI and Spike distance-based clustering solutions for three visual stimulus combinations. Dashed vertical lines are optimal cluster number for each. (F-H) Cluster similarity between ISI and SPIKE distance-based solutions for flash, chirp, and flash + chirp + color stimulus responses.

The ISI and SPIKE distance matrices were used to construct the cluster dendrogram using a hierarchical clustering algorithm (Fig. 1A-C) [7]. To estimate the correct number of clusters we examined two metrics; adjusted mutual information and the gap statistic. The gap statistic [34] estimates the optimum cluster number by comparing the dispersion of each cluster to the dispersion of a uniformly drawn sample. The number of clusters that produces the largest gap between these two dispersion values, taken across all clusters, is an estimate of the optimal number. Calculating the gap statistic of clustering solutions derived from ISI and SPIKE distance matrices for flash, chirp, and the combination of flash, chirp, and color responses (Fig. 1F-H), yielded optimal cluster numbers between 7 and 13 (Fig. 1D) – significantly lower than the 20-50 clusters expected based on prior work [5], [6], [7], [8], [9]. In contrast, the adjusted mutual information between the ISI-distance-based clustering solution and the solution for SPIKE distance peaked at 4, 21 and 35 for flash, chirp, and the combined three stimuli (Fig. 1E-H). We chose to use 35 as an optimal number of clusters for data obtained from wild type retinas based on a visual inspection of the clustered distance matrices and clustered response dissimilarity. Specifically, upon inspecting visual responses in Fig. 2, we found nontrivial differences between similar clusters (e.g., clusters 32-35) to support their separation (see also Fig. S1). Using

35 clusters yielded similar adjusted mutual information as the 21 cluster solution (Fig. 1e). While the 4 cluster solution in Figure 1e has higher mutual information, it is clear that the number of clusters should be higher. Generally speaking, our rationale in favoring a clustering solution with more clusters was twofold. First, consensus (mutual information) between ISI and spike-based strategies remains high indicating that such high cluster numbers meaningfully differentiate features in the data. Second, inappropriate splitting of a cluster - as becomes more likely with high cluster numbers - would only yield two clusters with the same filter. In contrast, inappropriate lumping of clusters would obscure the filter shapes of dissimilar clusters. Because we were interested in electrical filter differences, more clusters were preferred. Although the gap statistic is known to favor fewer clusters, it is only reduced from its peak value by about 25% for such high cluster numbers, indicating that the clustering solutions remain appropriately non-random.

Having determined an optimal number of clusters using mutual information, we next examined which stimulus and which distance metric to use for our final solution. We calculated the mutual information between clustering solutions using either flash or chirp as the visual stimulus. Comparing this mutual information score for SPIKE and ISI distance metrics, we found that the SPIKE distance metric had a higher score (not shown). Therefore, we chose to use the SPIKE metric for our final clustering solution. Finally, because we found that use of all three visual stimulus responses consistently yielded a higher number of clusters (Fig. 1E), all three were used for our final solution (Fig. 2).

Clustering revealed a range of transient and sustained ON and OFF subtypes with different levels of contrast and color preference (Fig. 2). Some of the clusters had few cells and noisy responses (clusters 3, 13, 18, 19, 21, 22, 31), indicating that the clustering algorithm was successful in separating these lower-quality data out into their own clusters. Similarly, clusters 11 and 20 only contained a single cell because that cell was poorly matched to other clusters.

For mouse retinal ganglion cells, the time course of eSTAs can often be sorted into one of four rough categories [22], [23], [38]. They can be either mono- or bi-phasic; and the deflection most closely preceding time zero can be either upward or downward (Fig. 2f). A downward deflection indicates that the average stimulus pulses preceding spikes were more negative (larger amplitude) than the mean stimulus of -800 mV. A notable nuance for eSTA interpretation is that an upward eSTA deflection does not indicate that the cell was activated purely by one or more low amplitude pulses, but rather than it was activated by a sequence of decreasing amplitude pulses, typically following multiple pulses of average or above average amplitude – the removal of moderate ongoing stimulation. Because a major goal of this work was to elaborate on previous reports that ON cells have upward deflecting eSTAs whereas OFF cells have downward deflecting eSTAs [22], we carefully examined this hypothesis in the present data. For each cluster in Figure 2F, we illustrated the smoothed, normalized eSTAs of individual cells (color traces), as well as the average of these normalized eSTAs in each cluster (thick black traces). We also calculated the average of the ON/OFF index for all clusters (numbers in Fig. 2B). Boundaries in the ON/OFF index are somewhat arbitrary, but we found that a lower cutoff of 0.12 captured most ON clusters and that an upper bound of -0.20 captured most OFF clusters for not only these clusters but also the 3 other cluster solutions presented below (Figs. 3, 5, and 6). Clusters between -0.20 and 0.12 were assumed to be ON-OFF cells. Based on these definitions, there were 17 ON clusters (49%), 13 OFF clusters (37%) and 5 ON-OFF clusters (14%) (Fig. 2B).

Of the 17 ON clusters in Fig. 2B, five had upward eSTAs (16, 30, 32-34) as expected, three had downward eSTAs (9, 13, 15), and nine had uncertain eSTAs (3, 7, 8, 12, 18, 19, 27, 29, 35) in Fig. 2F. These three downward eSTAs disagree with our hypothesis that ON cells have upward eSTAs; but each cluster could arguably have been assigned as ON-OFF clusters, instead. Of the 13 OFF clusters, only one (10) had an uncertain eSTA, with the remaining 12 having clear downward eSTAs (1, 2, 4-6, 14, 17, 20, 23-26). This agreed well with the previous assertion that OFF cells have downward eSTAs. Finally, of the 5 ON-OFF clusters, two had downward eSTAs (11 & 28) and 3 had uncertain eSTAs (21, 22, 31). In summary, all clusters with clearly upward eSTAs were classified as ON cells whereas all OFF cells had downward eSTAs in Fig. 2F.

We noted that for all ON clusters with uncertain eSTAs, the overlay of individual cells (Fig. 2F) showed a clear mix of upward and downward eSTAs (see also Fig. S2). This suggests either that the clusters were ‘dirty’ and contained multiple different cell types, or that the clusters represent true cell types that have no fixed association with a particular eSTA shape. To gain more insight on this issue, we chose to create an alternative clustering of the same data, but this time using the eSTA shape as the basis for cluster definitions.

B. Clustering RGCs per eSTAs Responses From Healthy Retinas

To assess the diversity of eSTAs more directly, we performed clustering based only on the shape of the eSTA using a similar hierarchical clustering algorithm. Computing the gap statistic from the pairwise distance matrix of normalized eSTAs for different cluster numbers showed a peak at 14. Hierarchical clustering of eSTAs divided them into 6 upward and 8 downward clusters (Fig. 3). Clusters 1 to 6 include monophasic and biphasic upward eSTAs. Clusters 7 to 14 have eSTAs with monophasic downward deflections of differing widths and latencies. As expected, we observed that the ON/OFF index was positive in the clusters with upward eSTA, indicating a large contribution of ON cells. Similarly, the ON/OFF index in 5 out of 8 clusters with downward deflection were negative, indicating the higher contribution of OFF cells in these clusters. As reflected in the low magnitude of their negative ON/OFF indices, most of these latter clusters also had significant ON responses suggesting heavy contamination by ON-OFF and possibly ON cells.

Looking more carefully at these eSTAs in the context of their visual cluster counterparts a few other details are of note (compare Fig. 3B to Fig. 2F). First, eSTA clusters 4, 5, and 6 (Fig. 3B) had narrow upward deflections that were preceded

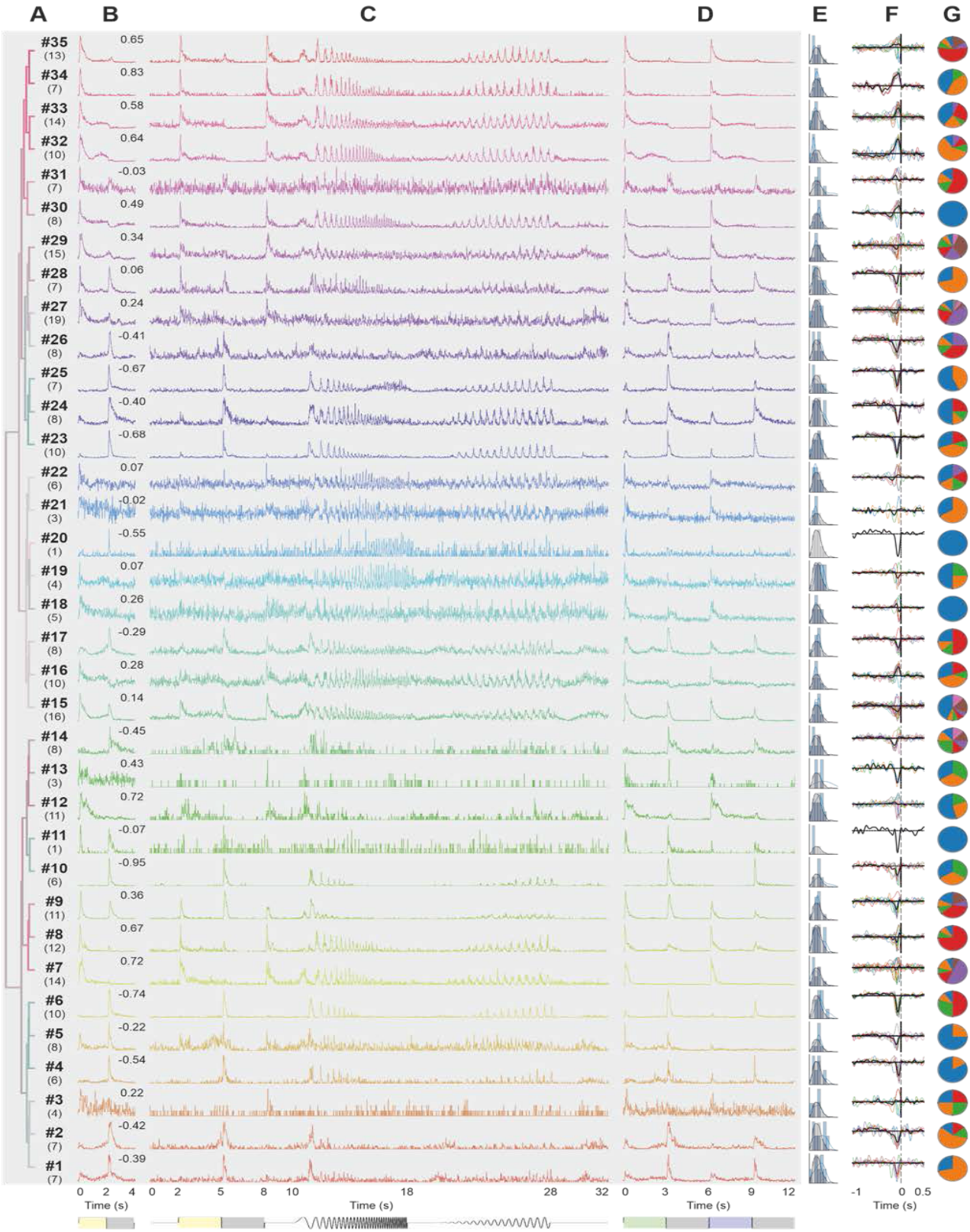

Fig. 2. **Clustering RGCs per visual responses from healthy retinas.** Timing of visual stimuli are represented at bottom. (A) Hierarchical clustering dendrogram. Each row represents a cluster. Cluster number (bold) and number of contributing cells (in parentheses) are listed for each cluster. (B) Peristimulus time histogram (PSTH) of responses to flash stimulus, averaged across all cells in each cluster. Inset numbers are ON/OFF indices for each cluster average (between -0.20 and 0.12 are ON-OFF, 0.12 and higher are ON, −0.20 and lower are OFF). (C) Average PSTH of chirp stimulus responses. (D) Average PSTH of color stimulus responses. Timing of color stimuli is indicated graphically at bottom of figure. (E) Distribution of direction selectivity indices for each cluster (blue) overlaid on the population distribution for all WT RGCs (grey). (F) Spike-triggered average of electrical stimuli (eSTA) for each cell in cluster (colored lines) and cluster average (thick black line). (G) Contribution of different retinas to each cluster indicating how broadly each cluster is represented within the population. Pie chart colors are re-assigned for each cluster. Grey box indicates stimuli used for clustering.

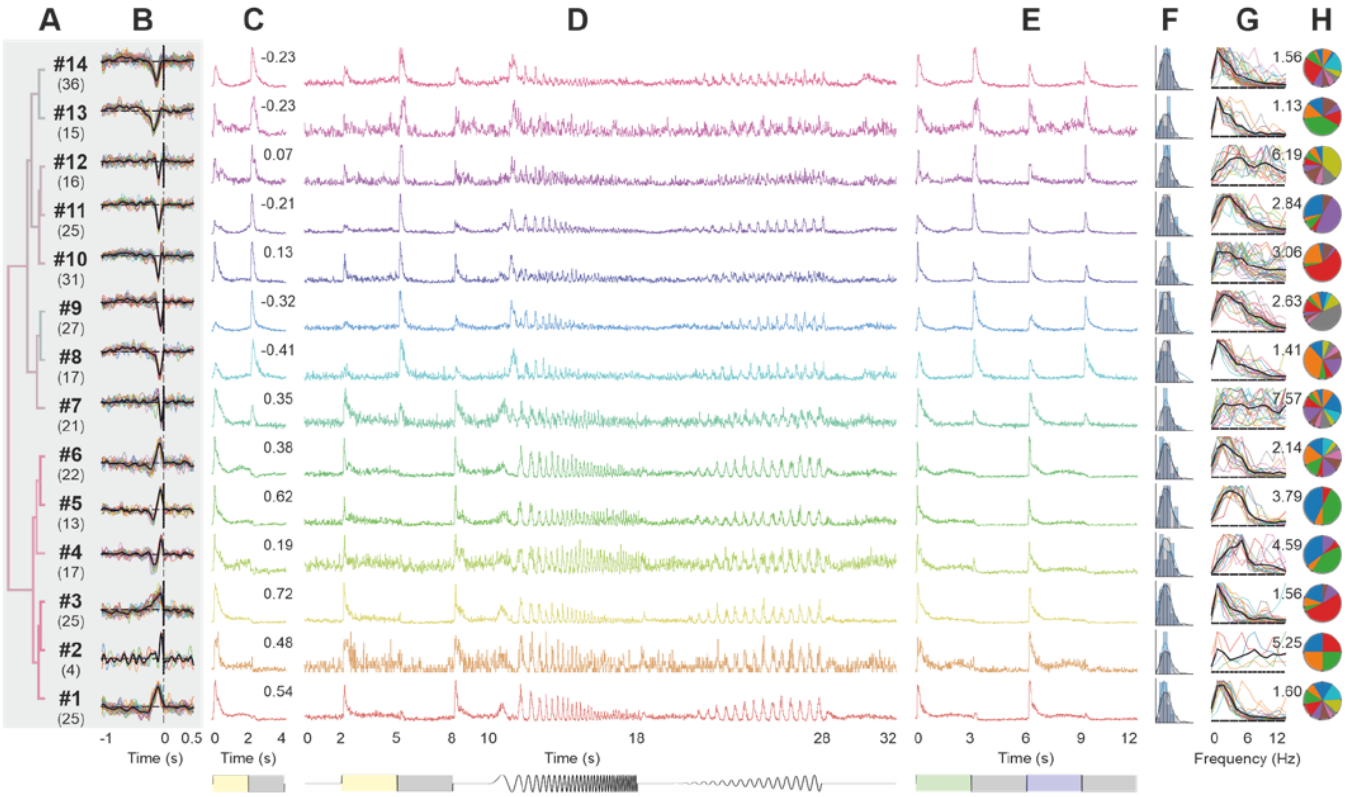

Fig. 3. **Clustering RGCs per eSTA responses from healthy retinas.** Figure conventions as in Figure 2. (A) Dendrogram with number and cell count for each cluster. (B) Contributing and average eSTAs. (C-E) Response PSTHs for flash, chirp, and color stimuli, respectively. (F) DSi distribution. (G) Power spectrum density (PSD) of eSTAs for contributing cells (colored lines) and cluster average (thick black line). Peak of average PSD (in Hz) is inset. (H) Fractional contribution to each cluster from different retinas.

by a weaker, narrow downward deflection. This indicates that these cells tended to spike following a fast alternation between downward and then upward electrical pulses. Put another way, the eSTA indicates that the cells prefer electrical alternations in the 2-5 Hz range as can be seen in the eSTA power spectrums found in Fig. 3G. Interestingly, looking back at Fig. 2F, we found no clusters with this pattern. However, we did find that the individual cells (thin colored lines in Fig. 2F) with this eSTA pattern were sorted into many different visual clusters (3, 5, 7, 8, 17-19, 21, 22, 27, 29, 35) – most of whom had indeterminate eSTA shapes due to averaging of multiple different shapes. Importantly, these visual clusters spanned the range of ON, OFF, and ON-OFF responses; however, the eSTA clusters 4, 5, and 6 were exclusively ON clusters. Thus, not only does electrical clustering sort cells with similar electrical preferences together, but it also groups cells with similar visual responses that were poorly clustered based purely on visual responses.

Second, examining the downward eSTAs of Fig. 3, we found that all biphasic downward eSTAs had a broad upward phase preceding the fast downward phase (8, 10, 13, 14). This contrasts with the narrow upward biphasic eSTAs discussed above. Whereas upward eSTAs 4 and 5 had bandpass-shaped power spectrums, these downward biphasic eSTAs had low-pass power spectrums mostly peaking below 2 Hz. Revisiting the visual clusters of Fig. 2, we also found this eSTA pattern for clusters 2, 6, 14, 15, 23, 26 – most of which were OFF clusters.

Taking these observations together, a picture emerges of a clear association between OFF cells with a downward, broad then narrow, biphasic eSTA pattern on the one hand and ON cells with an upward, narrow-narrow, biphasic eSTA pattern on the other hand. Detailed statistical analysis of these patterns follows.

So far, our analysis of the eSTAs for visual and electrical clusters has been somewhat subjective. To better quantify these differences, we also extracted features from the smoothed average of each of the cluster eSTAs shown in Figure 3. Extracted features were peak latency and width of the fast and slow deflections (Fig. S3). For the fastest deflection, both upward and downward eSTAs had similar latencies and widths ($p = 0.12$ and 0.34, respectively). For the slower deflections, both upward and downward eSTAs latencies tended to fall near one of two modes. Collectively, the slow deflection latencies were bimodal ($p = 0.044$) with downward eSTAs favoring long latencies and upward eSTAs favoring short latencies, although these differences were not significantly different due to this bimodality ($p = 0.19$). Although slower deflection widths exhibited a similar pattern with upward deflections favoring shorter widths, the small number of samples were neither significantly bimodal ($p = 0.81$) nor significantly different between upward and downward eSTAs ($p = 0.26$).

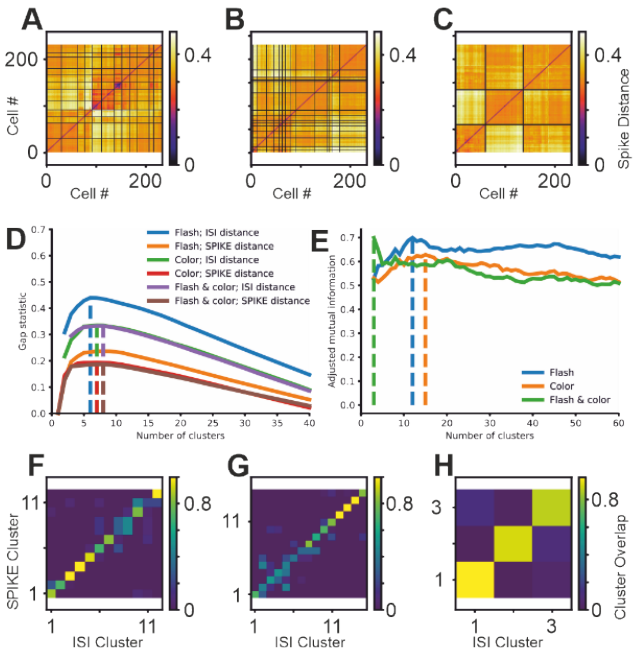

Fig. 4. **Optimization of RGC clusters from *rd*10 retinas** as in Figure 1. (A-C) Pairwise distance matrices for flash, color, and flash + color, respectively. (D) Scan of gap statistics across cluster number for these stimulus combinations paired with ISI and SPIKE distance metrics. (E) Mutual information between ISI and SPIKE for each stimulus combination. (F-H) Cluster similarity between ISI and SPIKE for flash, color, and flash + color, respectively.

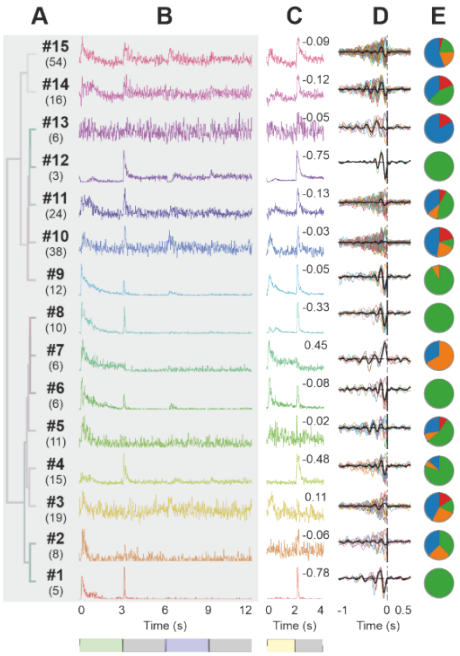

Fig. 5. **Clustering RGCs per Visual Responses from rd10 Retinas** as in Figure 2. (A) Dendrogram with number and cell count for each cluster. (B-C) Response PSTHs for color, and flash stimuli, respectively. Grey box indicates color stimuli were used for clustering. (D) eSTAs for contributing cells (colored lines) and cluster average (thick black line). (E) Fractional contribution to each cluster from different retinas.

When the subsets of these data that could be assigned to either ON or OFF visual categories were examined, these differences became more pronounced. Again, fast latencies

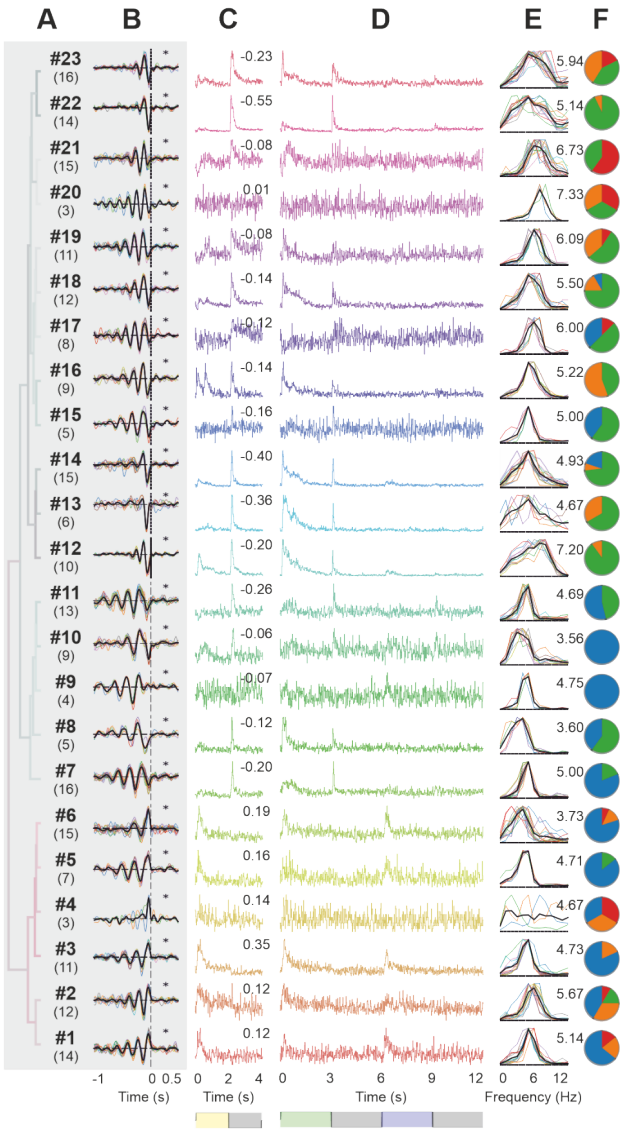

Fig. 6. **Clustering RGCs per eSTA responses from rd10 retinas** as in Fig. 2. (A) Dendrogram with number and cell count for each cluster. (B-C) eSTAs for contributing cells (colored lines) and cluster average (thick black line). (D) Response PSTHs for flash, and color stimuli, respectively. (E) PSD of eSTAs for contributing cells (colored lines) and cluster average (thick black line). (F) Fractional contribution to each cluster from different retinas.

and widths did not significantly differ between ON and OFF clusters ($p = 0.12$ and 0.74, respectively); however slow deflection latencies were slower ($p = 0.019$) for OFF clusters compared to ON clusters and, although not significant between ON and OFF clusters ($p = 0.11$) slow deflection widths were near bimodally distributed ($p = .052$) with a subset of broader widths for OFF clusters.

The duration - and for biphasic eSTAs the ratio – of an eSTA's deflection(s) reflects the cluster's temporal preference for electrical stimulation. Therefore, we further examined the eSTAs in frequency space to evaluate the similarity of these preferences. For each eSTA cluster, we computed the power spectrum density (PSD) of the eSTA using the Welch method (Fig. 3G). The peak frequency and the bandwidth of PSDs

were extracted for each cluster's eSTA. No significant difference was observed between the PSD properties of upward and downward eSTAs ($p = 0.36$ and 0.86 for peaks and bandwidths, respectively, Fig. S3).

C. Clustering RGC per Visual Responses From rd10 Retinas

Next, we evaluated RGC visual types and their e-STAs in rd10 degenerating retina. The extracellular activity of rd10 retinas at postnatal age 29 to 31 (P29 to 31) was evoked using the same electrical noise stimulus. We chose the rd10 model as a slower retinal degeneration model, resembling retinitis pigmentosa. Retinas aged P30 (in the middle of degeneration) were chosen so that enough visual responses would remain for some ganglion cells to be visually classified, while still characterizing electrical responses in unhealthy retina.

Chirp responses in initial rd10 experiments were weak and unreliable. Therefore, to optimize for high quality data collection, we used only flash and color stimuli for visual stimulation of the rd10 retina. Since most of the recorded units were poorly responsive to light, we did not apply the light response criteria for removing noisy data. The significance test of positive and negative eSTA deflections (ztest alpha=0.0001) [21] excluded all but 234 units from 4 retinas that were subsequently used for clustering. To find the optimal number of clusters we used the same approach as for healthy retinas where pairwise ISI and SPIKE distances were calculated (Fig. 4A-C). As before, the gap statistic (Fig. 4D) yielded a very low number of clusters. Therefore, the adjusted mutual information was used (Fig. 4E-H). It peaked at 12, 15, and 3 clusters for flash, color, and the combination of flash and color, respectively. As the highest number of clusters, we used the color stimulus-based solution of 15 clusters.

Most detected clusters were selective to the offset of the flash stimulus (Fig. 5). Whereas many of these clusters also contained ON responses, only cluster 7 was sufficiently dominated by ON responses to be classified as an ON cluster.

Clusters 1, 4, 8, and 12 were OFF, with the remaining clusters categorized as ON-OFF. Interestingly, whereas most clusters were dominated by OFF responses to monochromatic stimuli, ON responses to green light predominated, and only a few had responses to the onset of blue light.

As expected based on WT clusters, the OFF rd10 clusters had downward eSTAs. Likewise, ON cluster 7 had an upward eSTA. Most of the ON-OFF clusters had ambiguous eSTA shapes as the contributing cells had both upward and downward eSTAs. To get a better sense of how specific eSTA shapes relate to visual responses, we next clustered rd10 cells according to their eSTA shape.

D. Clustering RGC per eSTAs Responses From rd10 Retinas

The eSTAs of rd10 data were divided into 23 clusters using the same approach as for wild type eSTA data (Fig. 6). The gap statistic was used to estimate the optimal cluster number from agglomerative clustering based on the matrix of pairwise Euclidian distances between normalized eSTAs. In contrast to visual sorting of this data, the eSTA-sorted clusters had very low variability amongst eSTA shapes (compare single cell overlays between Fig. 5d and Fig. 6b). More surprisingly, electrical sorting revealed clusters with blue-ON, green-ON responses (Fig. 6; clusters 1, 3, 6, and possibly 2 and 5) where visual clustering (Fig. 5) was unable to reveal this pattern.

Examining these clusters in Figure 6, we found that all of them had multiphasic eSTAs with an oscillatory appearance – except for the low-quality cluster 4. In clusters where the eSTA oscillations were most pronounced (clusters 1-3, 5-11, 15-21), the visual responses were notably noisier. For the remaining 5 clusters, the eSTAs were downward; and visual responses were very clearly OFF (13, 14, 22, 23) or on the boundary with ON-OFF (12). In contrast, all five clusters with upward eSTAs (1)-3, 5-6) had a positive ON/OFF index. This alignment of upward eSTAs with ON clusters and downward eSTAs with OFF clusters matches the previously established pattern for WT cells. The remaining 13 clusters (4, 7-11, 15-21) were ON-OFF or only weakly fell into the ON and OFF categories. Additionally, they had oscillatory eSTAs with downward short-latency deflections; however, these deflections were seldom stronger than the preceding upward deflection. An exception to this latter observation was cluster 4 which appeared to be noisy due to a low cell count.

Digging into the first and second fastest deflections of these eSTAs (Fig. S4), we found very little variability between upward and downward eSTAs for first latency ($p = 0.37$) and width ($p = 0.34$), as well as second latency ($p = 0.78$) and width ($p = 0.69$). Likewise, there was no difference between ON and OFF cluster eSTAs for first latency ($p = 0.13$), first width ($p = 0.26$), second latency ($p = 0.99$) and second width ($p = 0.84$). Given these results, it is unsurprising that there were also no differences in PSD comparisons: upward vs. downward peak ($p = 0.16$) and bandwidth ($p = 0.60$), and ON vs. OFF peak ($p = 0.21$) and bandwidth ($p = 0.28$).

E. Comparing RGC Clusters From Healthy and rd10 Retinas

Comparing all healthy clusters with all rd10 clusters (Fig. 7), we found that whereas first eSTA deflection latency did not significantly differ ($p = 0.44$), first deflection width was significantly narrower for rd10 ($p = 0.044$) – likely owing to the influence of oscillatory spiking in shortening this deflection. As previously observed, second deflection latencies were bimodally distributed for healthy eSTAs ($p = 0.044$). The absence of the slower latencies in rd10 data led to a significant difference between healthy and rd10 clusters ($p < 0.0001$). Similarly, although not truly bimodal in distribution, the broader second eSTA deflection widths in healthy retina produced a significant difference in comparison with rd10 retina ($p = 0.0003$). Finally, the influence of oscillatory spiking in rd10 retinas resulted in higher PSD peaks ($p = 0.0003$) and narrower bandwidths ($p = 0.0015$) in comparison with healthy retinas.

F. Preliminary RGC Responses to Electrical Sinusoid

The experiments presented so far have aimed to identify unique electrical input filter shapes for the various RGC types.

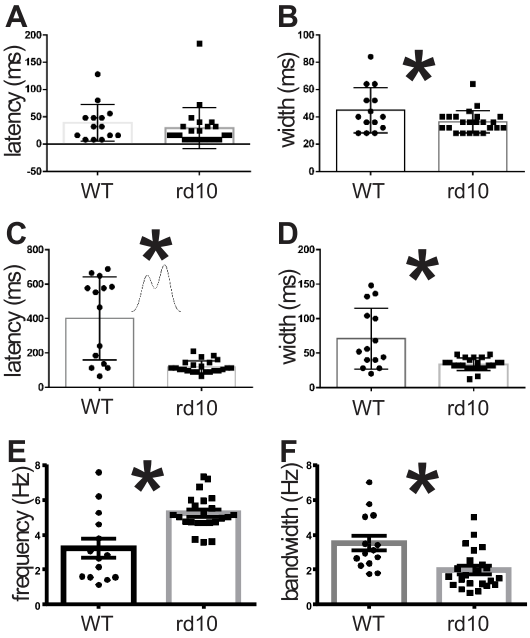

Fig. 7. **eSTA Parameters, WT vs. rd10** as in Fig. 4. (A-B) Distribution of first deflection latencies and widths, respectively. (C-D) Second deflection latency and width distributions, respectively. Inset in C illustrates bimodal distribution of WT second latencies. (E-F) Distribution of peak frequencies and bandwidths, respectively, of PSD from each cluster's eSTA. Asterisk (*) indicates a statistically significant unpaired t-test ($p < 0.05$).

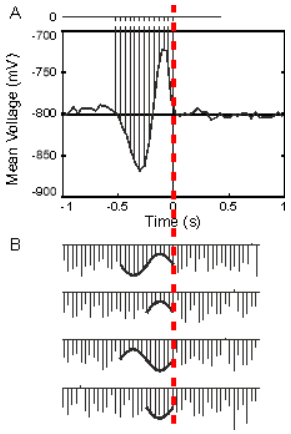

Fig. 8. **Selective stimulus design**. (A) The eSTA of a sample cell is discretized by a 25 Hz stimulus pulse train that can be approximated with a 2 Hz sine wave modulation. (B) Example 2 Hz full- and half-wave sinusoid stimuli embedded within ongoing 25 Hz cathodic pulse electrical noise. The first two (ending with upward modulation) are expected to preferentially activate ON RGCs and the second two (ending with downward modulation) are expected to activate OFF RGCs.

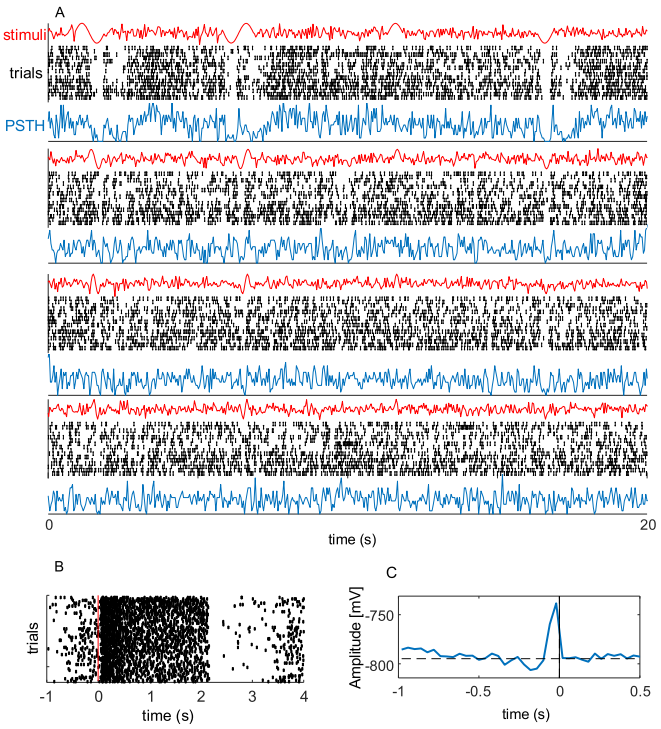

Fig. 9. **Example response to sinusoidal stimulation.** ON cell with upward biphasic eSTA, inhibited by slow downward sinusoids. (A) Noise embedded sinusoid pulse train envelope (red) with corresponding spike train rastergrams (black) and average response (blue). Sinusoids of 1, 2, 3, and 4 Hz are shown in rows 1-4, respectively. (B) Rastergram of spiking responses to 60 presentations of visual flash stimulus (2 s ON, then 2 s OFF). Vertical red line marks start of ON flash. (C) eSTA calculated from separate white noise stimulus.

By identifying such filters, we hoped to gain insight into electrical stimuli that could selectively activate individual RGC types. Separately, we have also begun experiments to test the selective stimulation hypothesis at a rudimentary level. Based on our earlier work [22], we developed a set of stimuli representing an idealized version of the eSTA shapes we had seen (Fig. 8). These stimuli consisted of a background noise stimulus like that used here, but with sinusoidal modulation imposed upon this noise at regular intervals. The sinusoids match the 4 basic shapes we have seen – upward and downward half sinusoids and down-up and up-down full sine waves. Furthermore, because we observed a range of frequency preferences in the eSTAs, we presented these 4 basic sinusoid shapes with the frequency of the sinusoid set at 1, 2, 3, and 4 Hz. Here we examine responses qualitatively from the perspective of the selective stimulation hypothesis.

Our primary hypothesis for selective electrical stimulation is that an upward deflection in electrical pulses should preferentially activate ON RGCs and a downward deflection should activate OFF RGCs. Among the 14 cells we have recorded with preferential sinusoid responses and clear eSTAs, the following patterns were noted.

We noted a collection of 5 ON cells that were suppressed by downward sinusoids of low frequency and had fast, biphasic upward eSTAs (Fig. 9, S5-S8). Although such suppression was not included in our original hypothesis formulation, suppression of ON cells by downward electrical sinusoid phases agrees with our selectivity hypothesis. In further agreement to this observation were 4 other ON cells with slow biphasic upward eSTAs. One was also inhibited by low frequency downward sinusoids (Fig. S9). One only responded to down-up sinusoids (Fig. S10). One was inhibited by down sinusoids and also responded to the lowest frequency down-up sinusoid (Fig. S11). The fourth responded both to down-up sinusoids and the end of down sinusoids in the manner of rebound excitation (Fig. S12).

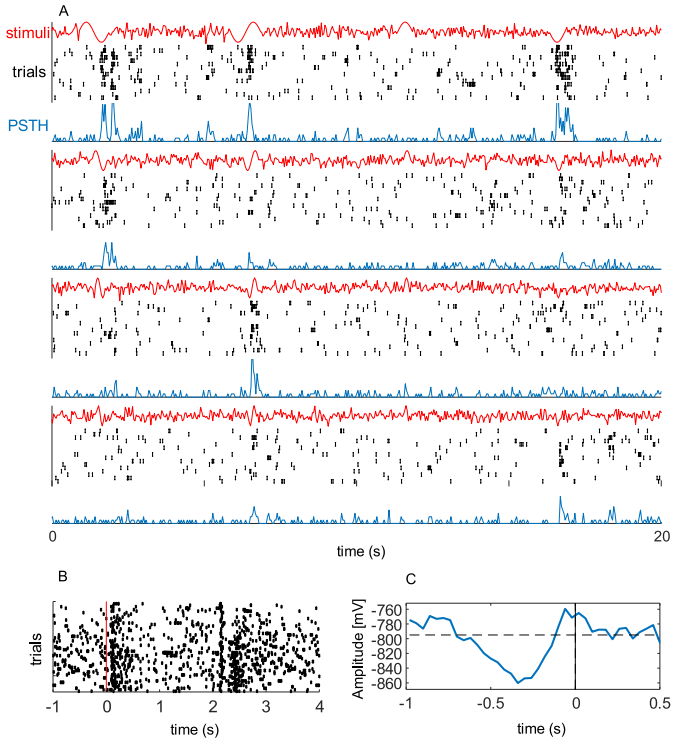

Fig. 10. **Example response to sinusoidal stimulation** as in Figure 9. ON-OFF cell (B) with triphasic downward-dominated eSTA (C), excited by downward sinusoids (A).

We also encountered 4 ON-OFF cells that responded to the downward phase of sinusoids (Fig. S12, S13-S15). Two had fast, monophasic eSTAs (Fig. S13, S14). The other two had strong, slow downward eSTAs (Fig. S15, 12), but one of those was unusual in being triphasic with preceding and following weak upward deflections (Fig. S12).

In this small pilot study, we did not encounter any clearly OFF cells with electrical responses. We did, however, encounter one cell which violated our hypothesis. It was an ON cell that responded weakly to some downward sinusoids and had a fast downward eSTA (Fig. S16). These preliminary observations suggest that the noise-embedded sinusoidal stimuli hold promise as a tool for probing RGC dynamics. Yet, to establish the validity and significance of these findings, larger-scale studies are essential. Future investigations with more data will be necessary to confirm the trends observed in this pilot study and to elucidate the mechanisms underlying the responses to these stimuli.

IV. Discussion

This work caps a series of experiments we have undertaken to better understand the relationship between a retinal neuron's visual and electrical response preferences. Our underlying purpose has been to refine the neural coding used in bionic vision through the development of RGC type-selective stimulation. In 2016, our group reported on a novel method to estimate the electrical stimulus preferences of retinal ganglion cells [21]. This method and variants upon it have since been used by other groups [23], [38], [39]. A year later, we followed our initial paper with a report on differences between electrical STAs for ON and OFF ganglion cells [22]. Since then, we reworked our visual stimulation protocol to implement the best-available differentiation of functional ganglion cell types in the mouse retina. Our goal was to elaborate on our previous papers and shed light on electrical stimuli specific to each of the dozens of ganglion cell types [20]. In our most recent elaboration attempt [24], we demonstrated the difficulties of connecting our spike train data to mouse cell types derived from calcium signal data and presented a preliminary sample of the limited diversity of eSTAs across these types. Finally, here, we present our most exhaustive examination of eSTA diversity to date, as it relates to visual responses. Rather than forcing our visual types to adhere to prior classification schemes, we have here optimized cell sorting according to the diversity of responses that is found in our own data. To gain additional insights, we have inverted the question and queried how visual responses differ when eSTA patterns are clustered instead; and we have also implemented these methods for degenerating rd10 retina. In both healthy and rd10 retinas, cells with ON visual responses tend to have upward deflecting eSTAs whereas OFF cells tend to have downward deflecting eSTAs and ON-OFF cells exhibit both up and down eSTAs. Leveraging these correspondences, we designed and tested a set of noise-embedded sinusoid stimuli reflecting many of the common eSTA shapes observed.

Many others have also examined this selective stimulation question with a range of methodologies and met with similarly qualified success [10], [13], [14], [15], [16], [17], [18], [19]. Despite these efforts, much work remains to identify selective electrical waveforms for enough of the retina's parallel information pathways to support detailed information coding in bionic vision.

In this study we not only validated our previous results but also report many new and valuable advances. To our knowledge, no other group has measured electrical input filters for so many visually-defined RGC types. Our examination of eSTAs in degenerating retina brings us closer to understanding how to relate knowledge from healthy retina to blind retina. In particular, eSTA-based sorting revealed visual response features that were not evident through visual sorting. It may be found that electrical responses in these degenerating cells are a more reliable way of identifying cell type. This also provides hope that electrical stimulation in blind retinas can be targeted according to RGC types in the absence of visual classification, thus leveraging the parallel pathways of normal vision for bionic sight.

A. On the Uncertainty of Cell Type Clustering

In this work, we have taken the view that the careful work of Baden et al. [9] is the most useful approximation to the theoretical full cohort of functionally differentiable RGCs in the mouse retina. They reported 32 RGC types clearly differentiated, with a small number of additional types suspected. Key to their work was an analysis of the tiling mosaics for each purported functional type. Such analysis describes close to the complete cohort of parallel visual information pathways of the retina – each of which completely samples from the full visual field. Our previous study using pseudo-calcium data

was an attempt to cleave as close as possible to this 'gold standard' while using MEA-recorded spike train data [24]. As noted, however, the pseudocalcium approach was found to be fundamentally flawed for the intended purpose.

Because the 'true' number of functional RGC types remains unresolved, the best approximation we currently achieve is to sort our data such that responses within cluster are very similar while differences between cluster responses are very different. Many algorithms exist to optimally balance these two competing goals; and improvement of such algorithms is an active domain of research unto its own right [40]. For data such as ours where multiple potential clustering solutions are equally valid, it helps to have an idea of the ideal number of clusters. In our case, that is 'a little bit more than 32'. Therefore, in Fig. 1 we chose the solution with 35 clusters, whereas in the other four clusterings, we chose the highest number of clusters from among the optimal solution candidates.

Improvements to clustering methodology are outside of our expertise; and we must rely on others in this respect. In contrast, we can work to improve the visual and electrical response data that is fed into the algorithms. To do this, we are continuing to investigate stimulus designs that produce very different responses for different functional cell types.

B. Lessons From Electrically-Based Clustering

We examined electrically-based clustering to more precisely characterize the properties of eSTA profiles and to evaluate their full diversity. Surprisingly, electrical clustering also revealed additional unexpected visual information. With electrical sorting, blue light responses were revealed for some clusters of ON cells that were not apparent using visual sorting. This suggests that type-specific electrical responses might deteriorate more slowly (if at all) than visual responses. Moreover, the modest success of electrical sorting in differentiating visual cell types raises the prospect that cell-type identification from purely electrical stimulation could be used after visual responses disappear during degeneration. Thus, proposed bidirectional retinal implants [41], [42] may be able to identify cell type so that the correct neural code is delivered to each cell. For example, formerly ON cells could be stimulated to produce ON-like spike trains, with OFF-stimulation delivered to formerly OFF cells. More work is needed to test this hypothesis that electrical responses alone can be used to identify RGC type.

It is also important to note, however, that relying solely on electrically-based clustering may conflate multiple visual response patterns. For example, the 35 WT clusters shown in Figure 2 are reduced to only 14 clusters in Figure 3, with clear visual response patterns lost (e.g., strongly green-OFF signals).

C. eSTA Oscillations in rd10 Mice

Degenerated retina differs from normal retina due to loss of photoreceptors, leading to changes in network activity patterns and eventual reorganization of the remaining cells [43]. An oscillatory spiking activity with a fundamental frequency in the 5-10 Hz range is a frequently reported consequence of photoreceptor loss in the degenerative retinal models, rd1 and rd10 [44], [45]. In our data, eSTAs obtained from rd10 retina carry an echo of these oscillations with frequency peaks ranging from 3 to 8 Hz – in agreement with previous reports for rd10 retina. The oscillations appear to be synchronized in phase by electrical stimulus sequences that elicit a response from the cell; but because phase and/or frequency vary slightly throughout the recording, this synchronization decays within the second of time shown in our eSTAs. In principle, it should be possible to remove the influence of oscillations from eSTAs such that the eSTA primarily reflects the average stimulus sequence that elicited spiking responses; however, this difficult task will require significant effort to complete. Until such corrections are made, we recommend caution in comparing eSTAs between healthy and rd10 retinas.

D. Selective Electrical Stimulation

We have included in this report early data on our attempts to selectively stimulate RGC types using 1, 2, 3, and 4Hz sinusoidal amplitude modulation of a 25 Hz pulse train, embedded within a background of white noise pulse amplitudes. Encouragingly, we found some cell types with differential responses to the probe sinusoids and present two examples in this paper. Amongst these few cells, most responses are in keeping with the hypothesis that upward sinusoid deflections should activate ON cells but not OFF cells, and that downward deflections should activate OFF cells, but not ON cells. Notable, however, is the diversity of responses which included pure spike train suppression and possibly rebound excitation in addition to immediate and delayed excitation. These data broaden our understanding of the relationship between visual cell type and electrical response; but are not yet sufficient either to reject our initial hypothesis or to guide a more sophisticated hypothesis for the dozens of true cell types that are understood to exist. Notably, a dearth of OFF cells prevented us from testing whether they are inhibited by upward deflections or activated by downward deflections.

From this pilot data, we have learned that a simple excitation model is insufficient to predict from the eSTA how cells will respond to electrical stimuli. Our hypothesis for visual type-selective electrical stimulation must be revised to incorporate neural phenomena like suppression and rebound excitation. Furthermore, the crude ON/OFF classification results in many different response patterns being attributed to ON, OFF, and ON-OFF RGC types. More complete visual characterization like that presented in the first part of this study may disambiguate this response diversity.

E. Other Considerations

MEA recording has some drawbacks. For example, identifying RGC types from fully degenerated rd10 retinas using MEA recordings is not possible. Therefore, we used the early stage of degeneration in rd10 mice (P29-31) to classify RGCs where some visual responses persist. Alternatively, this challenge can also be addressed by using whole-cell patch clamping recordings with dye injection. In this case, RGC classification

is based on dendritic tree stratification and other morphological properties. Another advantage of patch clamping is that it can capture nonlinearities internal to the cell that are not evident with extracellular recordings. In this context, the eSTA clusters provide an alternative framework that allows us to uncover response patterns that might be obscured by the degeneration of visual responses.

For eSTA estimation, we excluded spikes occurring during the first 10 ms. Our rationale is that this eliminates the potential eSTA contribution of both stimulation artifacts and spikes that result from direct electrical activation of the RGC – with only limited reduction of 'indirect' spikes (discussed further in [20]). This exclusion allows us to estimate the eSTA for the indirect stimulation of RGCs via the retinal network. Additionally, the mean amplitude of the noise stimulus has been optimized to activate the retinal network through temporal integration of multiple pulses – in contrast to the single pulse activation that has been traditionally investigated (an approach we have termed 'tickling the retina'; described in [21] and discussed further in [22]). In the present data, we report eSTA latencies of less than 10 ms, despite discarding spike with latencies below 10 ms. This is a known artifact of splining our data. Accordingly, the latencies reported here should be interpreted as only approximate. Nevertheless, they are useful as we have presented them – for comparisons between first and second eSTA deflections, between RGC cluster types, and between WT and rd10 eSTAs.

F. Future Work

There is great difficulty in collecting enough recordings with enough data from each recording to support nuanced classification of both visual and electrical response properties. Calcium imaging is one method of recording from enough cells; however, our ability to match calcium activity with spike trains remains incomplete (discussed in [24]). To remain useful for a bidirectional visual prosthesis [39], [40], MEA-based recordings remain the best way to collect data from thousands of cells.

In this work, compromises were made to accommodate simultaneous recording from dozens of cells spread over a large area. As a result, the stimuli were not optimized for individual cells. Going forward, visual stimuli could be optimized to better differentiate between the known color-selective cell types as well as the range of direction- and orientation-selective cell types. In both cases, optimal selectivity is achieved when center and surround of a cell's receptive field are differentially stimulated.

Regarding electrical stimulation, the eSTA is a rough estimate of the theoretical electrical input filter applied by each cell to incoming stimulation, however this estimate could be refined significantly. For example, we believe it may be possible to reveal various components of the retinal circuitry with a sufficiently detailed eSTA [20]. To do this, it will be necessary to present a current-controlled, time-varying stimulus without artifacts obscuring the recorded spike train. Such methods are available [39], but remain difficult to implement for the collection of thousands of data points for long recording times. Additionally, the amplitude and spectral statistics of such stimuli must be carefully optimized to fully reveal all components of a cell's electrical responsiveness. Moreover, the network elements giving rise to the eSTA remain unclear. To date, there is ambiguity about which cells and synapses underlie the eSTAs that we have reported. Differences between the time course of eSTAs reported here and Sekhar et al. [21], as well as between our lab's eSTAs and those of other labs [23], [38], [39] suggest that multiple circuit elements can be activated to elicit RGC eSTAs. Previously, we proposed a theoretical framework for how these mechanisms may interact [20]. We and others continue to pursue the use of pharmacological agents and transgenic mice to better understand eSTAs. Another caveat remains that the STA method employed here reveals even the faintest correlations between electrical stimulus and response. Our initial attempts to computationally model the electrical sensitivity of RGCs to support optimal stimulus design have revealed high variability in responses to the stimuli presented here [46]. To better support bionic vision, it may be necessary to improve this stimulus response correlation during electrical noise stimulation.

Early data from our attempt to achieve selective RGC type stimulation using sinusoidal pulse modulation are encouraging. However, they further emphasize the need to refine visual and electrical characterization stimuli so that the full set of RGC types can be differentiated. Such refinements must yield a compact tool that can be included in selective stimulation experiments alongside the main stimuli without requiring excessive experimental recording durations. Ultimately, these initial attempts to connect visual RGC types with characteristic electrical stimulation patterns has been limited to only the coarsest ON and OFF types. Whether or not visual-electrical correspondences exist for more precisely defined RGC types remains to be demonstrated.

Author Contributions

Hamed Shabani and Zohreh Hosseinzadeh performed the experiments. Hamed Shabani, Eberhart Zrenner, Daniel L. Rathbun, and Zohreh Hosseinzadeh interpreted the results. Hamed Shabani, Daniel L. Rathbun, and Zohreh Hosseinzadeh designed the study and drafted the manuscript. All authors corrected and approved the final version of the manuscript.

Data Availability

The data that support the findings of this study are openly available in Zenodo at https://doi.org/10.5281/zenodo.6819514

References

[1] L. N. Ayton et al., "An update on retinal prostheses," *Clin. Neurophysiol.*, vol. 131, no. 6, pp. 1383–1398, Jun. 2020.

[2] M. S. Humayun et al., "Interim results from the international trial of second sight's visual prosthesis," *Ophthalmology*, vol. 119, no. 4, pp. 779–788, Apr. 2012.

[3] M. Keserü et al., "Acute electrical stimulation of the human retina with an epiretinal electrode array," *Acta Ophthalmologica*, vol. 90, no. 1, pp. 1–8, Feb. 2012.

[4] K. Stingl et al., "Interim results of a multicenter trial with the new electronic subretinal implant alpha AMS in 15 patients blind from inherited retinal degenerations," *Frontiers Neurosci.*, vol. 11, p. 445, Aug. 2017.

[5] J. A. Bae et al., "Digital museum of retinal ganglion cells with dense anatomy and physiology," *Cell*, vol. 173, no. 5, pp. 1293–1306, May 2018.

[6] B. A. Rheaume et al., "Single cell transcriptome profiling of retinal ganglion cells identifies cellular subtypes," *Nature Commun.*, vol. 9, no. 1, pp. 1–7, Jul. 2018.

[7] J. Jouty, G. Hilgen, E. Sernagor, and M. H. Hennig, "Non-parametric physiological classification of retinal ganglion cells in the mouse retina," *Frontiers Cellular Neurosci.*, vol. 12, p. 481, Dec. 2018.

[8] N. M. Tran et al., "Single-cell profiles of retinal ganglion cells differing in resilience to injury reveal neuroprotective genes," *Neuron*, vol. 104, no. 6, pp. 1039–1055, Dec. 2019.

[9] T. Baden, P. Berens, K. Franke, M. R. Rosón, M. Bethge, and T. Euler, "The functional diversity of retinal ganglion cells in the mouse," *Nature*, vol. 529, no. 7586, pp. 345–350, Jan. 2016.

[10] P. Twyford and S. Fried, "The retinal response to sinusoidal electrical stimulation," *IEEE Trans. Neural Syst. Rehabil. Eng.*, vol. 24, no. 4, pp. 413–423, Apr. 2016.

[11] D. K. Freeman, D. K. Eddington, J. F. Rizzo, and S. I. Fried, "Selective activation of neuronal targets with sinusoidal electric stimulation," *J. Neurophysiol.*, vol. 104, no. 5, pp. 2778–2791, Nov. 2010.

[12] P. Twyford, C. Cai, and S. Fried, "Differential responses to high-frequency electrical stimulation in ON and OFF retinal ganglion cells," *J. Neural Eng.*, vol. 11, no. 2, Feb. 2014, Art. no. 025001.

[13] T. Guo et al., "Selective activation of ON and OFF retinal ganglion cells to high-frequency electrical stimulation: A computational modeling study," in *Proc. 36th Ann. Int. Con. IEEE Eng. Med. Biol. Soc.*, Aug. 2014, pp. 6108–6111.

[14] G. Goetz et al., "Contrast sensitivity with a subretinal prosthesis and implications for efficient delivery of visual information," *Investigative Opthalmol. Vis. Sci.*, vol. 56, no. 12, pp. 7186–7194, Nov. 2015.

[15] M. Im and S. I. Fried, "Temporal properties of network-mediated responses to repetitive stimuli are dependent upon retinal ganglion cell type," *J. Neural Eng.*, vol. 13, no. 2, Feb. 2016, Art. no. 025002.

[16] W. Qin et al., "Single-compartment models of retinal ganglion cells with different electrophysiologies," *Network, Comput. Neural Syst.*, vol. 28, nos. 2–4, pp. 74–93, Oct. 2017.

[17] M. Im, P. Werginz, and S. I. Fried, "Electric stimulus duration alters network-mediated responses depending on retinal ganglion cell type," *J. Neural Eng.*, vol. 15, no. 3, Mar. 2018, Art. no. 036010.

[18] T. Guo et al., "Closed-loop efficient searching of optimal electrical stimulation parameters for preferential excitation of retinal ganglion cells," *Frontiers Neurosci.*, vol. 12, p. 168, Mar. 2018.

[19] J. Oesterle et al., "Bayesian inference for biophysical neuron models enables stimulus optimization for retinal neuroprosthetics," *eLife*, vol. 9, Oct. 2020, Art. no. e54997.

[20] D. L. Rathbun, N. Ghorbani, H. Shabani, E. Zrenner, and Z. Hosseinzadeh, "Spike-triggered average electrical stimuli as input filters for bionic vision—A perspective," *J. Neural Eng.*, vol. 15, no. 6, Oct. 2018, Art. no. 063002.

[21] S. Sekhar, A. Jalligampala, E. Zrenner, and D. L. Rathbun, "Tickling the retina: Integration of subthreshold electrical pulses can activate retinal neurons," *J. Neural Eng.*, vol. 13, no. 4, May 2016, Art. no. 046004.

[22] S. Sekhar, A. Jalligampala, E. Zrenner, and D. L. Rathbun, "Correspondence between visual and electrical input filters of ON and OFF mouse retinal ganglion cells," *J. Neural Eng.*, vol. 14, no. 4, Jun. 2017, Art. no. 046017.

[23] E. Ho et al., "Spatiotemporal characteristics of retinal response to network-mediated photovoltaic stimulation," *J. Neurophysiol.*, vol. 119, no. 2, pp. 389–400, Feb. 2018.

[24] H. Shabani, M. Sadeghi, E. Zrenner, D. L. Rathbun, and Z. Hosseinzadeh, "Classification of pseudocalcium visual responses from mouse retinal ganglion cells," *Vis. Neurosci.*, vol. 38, p. E016, Nov. 2021.

[25] A. Jalligampala, S. Sekhar, E. Zrenner, and D. L. Rathbun, "Optimal voltage stimulation parameters for network-mediated responses in wild type and rd10 mouse retinal ganglion cells," *J. Neural Eng.*, vol. 14, no. 2, Feb. 2017, Art. no. 026004.

[26] M. Meister, J. Pine, and D. A. Baylor, "Multi-neuronal signals from the retina: Acquisition and analysis," *J. Neurosci. Methods*, vol. 51, no. 1, pp. 95–106, Jan. 1994.

[27] H. Shabani, "Classifying retinal ganglion cells for bionic vision," Ph.D. dissertation, Inst. Ophthalmic Res., Univ. Tuebingen, Tuebingen, Germany, 2021.

[28] M. Sadeghi, "Spike based mouse retinal ganglion cell classification for a potential toolbox," M.S. thesis, Inst. Ophthalmic Res., Univ. Tuebingen, Tuebingen, Germany, 2018.

[29] T. Kreuz, J. S. Haas, A. Morelli, H. D. I. Abarbanel, and A. Politi, "Measuring spike train synchrony," *J. Neurosci. Methods*, vol. 165, no. 1, pp. 151–161, Sep. 2007.

[30] T. Kreuz, D. Chicharro, M. Greschner, and R. G. Andrzejak, "Time-resolved and time-scale adaptive measures of spike train synchrony," *J. Neurosci. Methods*, vol. 195, no. 1, pp. 92–106, Jan. 2011.

[31] T. Kreuz, D. Chicharro, C. Houghton, R. G. Andrzejak, and F. Mormann, "Monitoring spike train synchrony," *J. Neurophysiol.*, vol. 109, no. 5, pp. 1457–1472, Mar. 2013.

[32] M. Mulansky and T. Kreuz, "PySpike—A Python library for analyzing spike train synchrony," *SoftwareX*, vol. 5, pp. 183–189, 2016.

[33] E. Jones, T. Oliphant, and P. Peterson. (2001). *SciPy: Open Source Scientific Tools for Python*. [Online]. Available: https://scipy.org/

[34] R. Tibshirani, G. Walther, and T. Hastie, "Estimating the number of clusters in a data set via the gap statistic," *J. Roy. Stat. Soc., B, Stat. Methodol.*, vol. 63, no. 2, pp. 411–423, May 2001.

[35] T. Sharpee, N. C. Rust, and W. Bialek, "Analyzing neural responses to natural signals: Maximally informative dimensions," *Neural Comput.*, vol. 16, no. 2, pp. 223–250, Feb. 2004.

[36] R. S. Williamson, M. Sahani, and J. W. Pillow, "The equivalence of information-theoretic and likelihood-based methods for neural dimensionality reduction," *PLOS Comput. Biol.*, vol. 11, no. 4, Apr. 2015, Art. no. e1004141.

[37] S. I. Fried, H. A. Hsueh, and F. S. Werblin, "A method for generating precise temporal patterns of retinal spiking using prosthetic stimulation," *J. Neurophysiol.*, vol. 95, no. 2, pp. 970–978, Feb. 2006.

[38] M. I. Maturana et al., "Electrical receptive fields of retinal ganglion cells: Influence of presynaptic neurons," *PLOS Comput. Biol.*, vol. 14, no. 2, Feb. 2018, Art. no. e1005997.

[39] L. Höfling, J. Oesterle, P. Berens, and G. Zeck, "Probing and predicting ganglion cell responses to smooth electrical stimulation in healthy and blind mouse retina," *Sci. Rep.*, vol. 10, no. 1, pp. 1–20, Mar. 2020.

[40] D. Xu and Y. Tian, "A comprehensive survey of clustering algorithms," *Ann. Data Sci.*, vol. 2, no. 2, pp. 165–193, Jun. 2015.

[41] V. Rincón Montes et al., "Toward a bidirectional communication between retinal cells and a prosthetic device—A proof of concept," *Frontiers Neurosci.*, vol. 13, p. 367, Apr. 2019.

[42] N. P. Shah and E. J. Chichilnisky, "Computational challenges and opportunities for a bi-directional artificial retina," *J. Neural Eng.*, vol. 17, no. 5, Oct. 2020, Art. no. 055002.

[43] B. W. Jones, M. Kondo, H. Terasaki, Y. Lin, M. McCall, and R. E. Marc, "Retinal remodeling," *Jpn. J. Ophthalmol.*, vol. 56, no. 4, pp. 289–306, Jul. 2012.

[44] Y. S. Goo, D. J. Park, J. R. Ahn, and S. S. Senok, "Spontaneous oscillatory rhythms in the degenerating mouse retina modulate retinal ganglion cell responses to electrical stimulation," *Frontiers Cellular Neurosci.*, vol. 9, pp. 512–519, Jan. 2016.

[45] S. F. Stasheff, M. Shankar, and M. P. Andrews, "Developmental time course distinguishes changes in spontaneous and light-evoked retinal ganglion cell activity in rd1 and rd10 mice," *J. Neurophysiol.*, vol. 105, no. 6, pp. 3002–3009, Jun. 2011.

[46] S. Sekhar, P. Ramesh, G. Bassetto, E. Zrenner, J. H. Macke, and D. L. Rathbun, "Characterizing retinal ganglion cell responses to electrical stimulation using generalized linear models," *Frontiers Neurosci.*, vol. 14, p. 378, May 2020.